HEALTH AND MEDICINE

ROS-responsive chitosan-SS31 prodrug for AKI therapy via rapid distribution in the kidney and long-term retention in the renal tubule

Di Liu[1], Gaofeng Shu[1], Feiyang Jin[1], Jing Qi[1], Xiaoling Xu[1], Yan Du[1], Hui Yu[1], Jun Wang[1], Mingchen Sun[1], Yuchan You[1], Minxia Zhu[1], Meixuan Chen[1], Luwen Zhu[1], Qiying Shen[1], Xiaoying Ying[1], Xuefang Lou[3]*, Saiping Jiang[2]*, Yongzhong Du[1]*

The development of drugs with rapid distribution in the kidney and long-term retention in the renal tubule is a breakthrough for enhanced treatment of acute kidney injury (AKI). Here, L-serine–modified chitosan (SC) was synthesized as a potential AKI kidney–targeting agent due to the native cationic property of chitosan and specific interaction between kidney injury molecule–1 (Kim-1) and serine. Results indicated that SC was rapidly accumulated and long-term retained in ischemia-reperfusion–induced AKI kidneys, especially in renal tubules, which was possibly due to the specific interactions between SC and Kim-1. SC-TK-SS31 was then prepared by conjugating SS31, a mitochondria-targeted antioxidant, to SC via reactive oxygen species (ROS)–sensitive thioketal linker. Because of the effective renal distribution combined with ROS-responsive drug release behavior, the administration of SC-TK-SS31 led to an enhanced therapeutic effect of SS31 by protecting mitochondria from damage and reducing the oxidative stress, inflammation, and cell apoptosis.

INTRODUCTION

Acute kidney injury (AKI) manifests as a rapid decline in renal function with increased morbidity and mortality (*1*). The main causes of AKI include kidney ischemia-reperfusion (IR) injury, sepsis, and nephrotoxins (*2*, *3*). The incidence of AKI has been rising, causing increased risks of chronic kidney disease and end-stage renal disease (*1*, *4*). Despite advance in therapeutic strategies, AKI remains an independent predictor of in-hospital mortality (*5*).

The pathogenesis of AKI is complicated with various mechanisms, including oxidative stress, inflammation, vascular damage, and so on (*6*, *7*). Among them, oxidative stress is considered as the central aggravating factor (*8*). Reactive oxygen species (ROS) have been well reported to be associated with AKI, and the dysregulation of ROS can trigger the pathways toward cellular apoptosis, necrosis, and renal fibrosis (*9*). Mitochondria can be easily damaged during AKI process because they are the major intracellular source of ROS (*10*). D-Arg-dimethylTyr-Lys-Phe-NH_2 (SS31) is a promising peptide-based drug for the treatment of AKI due to its mitochondrial targeting ability and excellent antioxidative property (*11*, *12*). Cardiolipin is a unique phospholipid exclusively expressed on the inner mitochondrial membrane, which is essential for the formation of cristae and the organization of the respiratory complexes into supercomplexes for optimal oxidative phosphorylation (*12*). SS31 can protect mitochondrial cristae from damage and promotes oxidative phosphorylation by selectively binding with cardiolipin via electrostatic and hydrophobic interactions, thereby playing an important role in the treatment of AKI (*12*). Previous studies have demonstrated that SS31 can protect the kidney from oxidative-associated injury including IR-induced AKI (*11*) and age-associated glomerular architecture changes (*13*). However, for SS31, there are many factors limiting the bioavailability of peptide-based therapeutics including systemic proteases, rapid metabolism, opsonization, conformational changes, dissociation, noncovalent complexation with blood products, and destruction of labile side groups (*14*), ultimately resulting in poor treatment efficiency.

With the rapid development of prodrug design (*15*), effective delivery to the kidney assisted by renal targeting drug carriers is a potential strategy to improve the therapeutic efficacy of AKI. Tubular epithelial cell (TEC) death caused by ischemic, toxic, septic, or obstructive insults is the most common cause of AKI (*16*), and therefore, renal tubules is an ideal targeting area for AKI therapy. To target its cargo to the renal tubule, a drug carrier needs to pass anatomical barriers between the circulation and the tubular cell, including endothelial fenestrations and glomerular basement membrane (GBM). Because of the negatively charged heparin sulfate contained in the fenestrae and the presence of negatively charged sulfated glycosaminoglycans in the GBM, positively charged macromolecules and particles will be transported more easily than negatively charged drug carriers (*17*). Chitosan is a native cationic polysaccharide with a pK_a (where K_a is the acid dissociation constant) of being around 6.5 to 7.0 (*18*) and with excellent biocompatibility and biodegradation (*19*), which makes it a potential kidney-targeted drug carrier. Chemical modification of macromolecules is used to generate materials with fascinating physiochemical and biochemical properties for biomedical applications. L-Serine is a potent renal tubule–targeted modifier (*20*), which is also a potential targeting agent for kidney injury molecule–1 (Kim-1). Kim-1 is a transmembrane protein markedly up-regulated in injured kidneys, particularly renal proximal tubules, which induces the internalization and, therefore, the clearance of dead cells through the recognition of phosphatidylserine and oxidized lipoprotein on the surfaces of the dead cells (*21*). Serine is the substantial structure for interaction with Kim-1 in the process of endocytosis (*22*). Therefore, L-serine–modified chitosan

[1]Institute of Pharmaceutics, College of Pharmaceutical Sciences, Zhejiang University, 866 Yu-Hang-Tang Road, Hangzhou 310058, China. [2]Department of Pharmacy, The First Affiliated Hospital, College of Medicine, Zhejiang University, 79 Qingchun Road, Hangzhou 310003, China. [3]School of Medicine, Zhejiang University City College, Hangzhou 310015, China.
*Corresponding author. Email: duyongzhong@zju.edu.cn (Y.D.); j5145@zju.edu.cn (S.J.); louxf@zucc.edu.cn (X.L.)

(SC) as the drug carrier was designed in our study, expecting that it can effectively accumulate in renal tubules, and well internalized by TECs mediated by Kim-1.

Here, we designed the AKI kidney–targeted prodrug (SC-TK-SS31) by combining SS31 with SC via thioketal (TK) bond, an attractive ROS-sensitive linker (*23*, *24*), for effective therapy of AKI (Fig. 1). The accumulation and retention of SC-TK-SS31 in injured renal tubules allow for the enhancement of therapeutic effect of SS31. The combination of renal tubule-targeted carries and mitochondria-targeted antioxidant is previously unidentified and valuable for the treatment of AKI. The chemical structure, targeted biodistribution, targeted cellular uptake, and drug release behavior of SC-TK-SS31 were evaluated. Both in vitro and in vivo experiments were performed to evaluate the therapeutic potential of SC-TK-SS31 to prevent AKI.

RESULTS

Syntheses and characteristics of chitosan-based carriers

We first designed three types of chitosan-based carriers as the candidates for AKI kidney–targeted drug delivery, including L-serine–modified chitosan (SC), oligolysine polyethylene glycol–modified chitosan (PEG-C), and L-serine–modified PEG-C (S-PEG-C). The synthetic routes of SC, PEG-C, and S-PEG-C were illustrated in fig. S1. For SC synthesis, boc–L-Ser(tBu)–OH–modified chitosan (preSC) was firstly prepared by constructing boc–L-Ser(tBu)–OH (preSer) on the amino groups of chitosan, followed by the deprotection of *tert*-butyloxy carbonyl (boc) and *tert*-butyl (tBu) groups via trifluoroacetic acid (TFA) cocktail treatment. The chemical structures of preSC and SC were analyzed by ^{1}H nuclear magnetic resonance (^{1}H NMR) spectrum (fig. S2). It was found that preSC had the characteristic signals of preSer at ~1.1 and ~1.4 parts per million (ppm), which belonged to the boc and tBu group, respectively. On the other hand, the peaks at ~1.1 and ~1.4 ppm disappeared after TFA cocktail treatment, representing the successful deprotection of boc and tBu group. This result suggested that SC was successfully prepared in our study. The molecular weight of SC measured by gel permeation chromatography (GPC) was 2.84 kDa (fig. S3). The substitution ratio of serine in SC was calculated to be about 4/1 (serine/C, mol/mol). PEG-C and S-PEG-C were also prepared by amidation reaction method. The ^{1}H NMR spectrum revealed that the characteristic peaks of PEG at 3.37 to 3.83 ppm appeared in the spectrum of PEG-C and preSer-PEG-C, indicating the successful synthesis of PEG-C and S-PEG-C.

Screening of AKI kidney–targeted carriers

In vivo distribution experiments were carried out to evaluate the renal targeting efficacy of different chitosan-based carriers (Fig. 2, A to D). Before administration, a commercial fluorescent dye of Cy5 was used to label the chitosan skeleton (C), SC, PEG-C, and S-PEG-C, which was abbreviated as Cy5-C, Cy5-SC, Cy5-PEG-C, and Cy5-S-PEG-C, respectively. Fluorescence images of major organs obtained from the normal and AKI mice were captured at a predetermined time (4 and 12 hours) after intravenous injection of Cy5-labeled carries. As shown in Fig. 2 (B and C), the normal mice displayed relatively weak fluorescent signals in the lung and kidney at 4 hours after administration of Cy5-C. The healthy mice treated with Cy5-PEG-C and Cy5-S-PEG-C had a relatively higher florescence intensity in the liver than

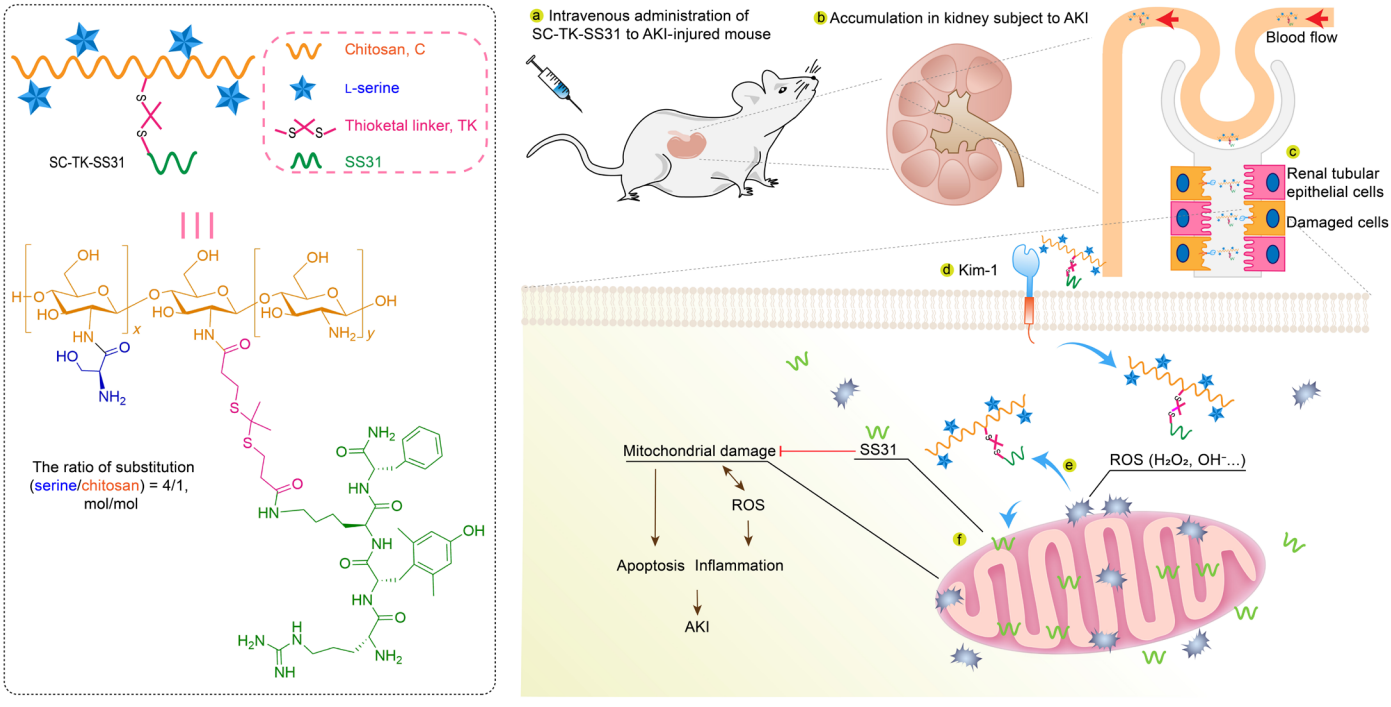

Fig. 1. Chemical structure of SC-TK-SS31 and the schematic illustration showing the relief of AKI by SC-TK-SS31. After intravenous administration, SC-TK-SS31 stays stably during delivery in blood circulation and accumulates in renal tubules of the kidney subject to AKI. Specifically expressed Kim-1 in injured TECs is associated with the internalization of SC-TK-SS31. Epithelial cell injury in AKI is characterized by increased formation of ROS. Mitochondria, as the major sites of ROS production, are first damaged and urgent for protection. ROS triggers the release of SS31 via cleavage of ROS-sensitive TK linker, therefore preventing the mitochondria damage and decreasing ROS production. The alleviation of oxidative stress further diminishes inflammation and apoptosis of TECs, thereby relieves AKI.

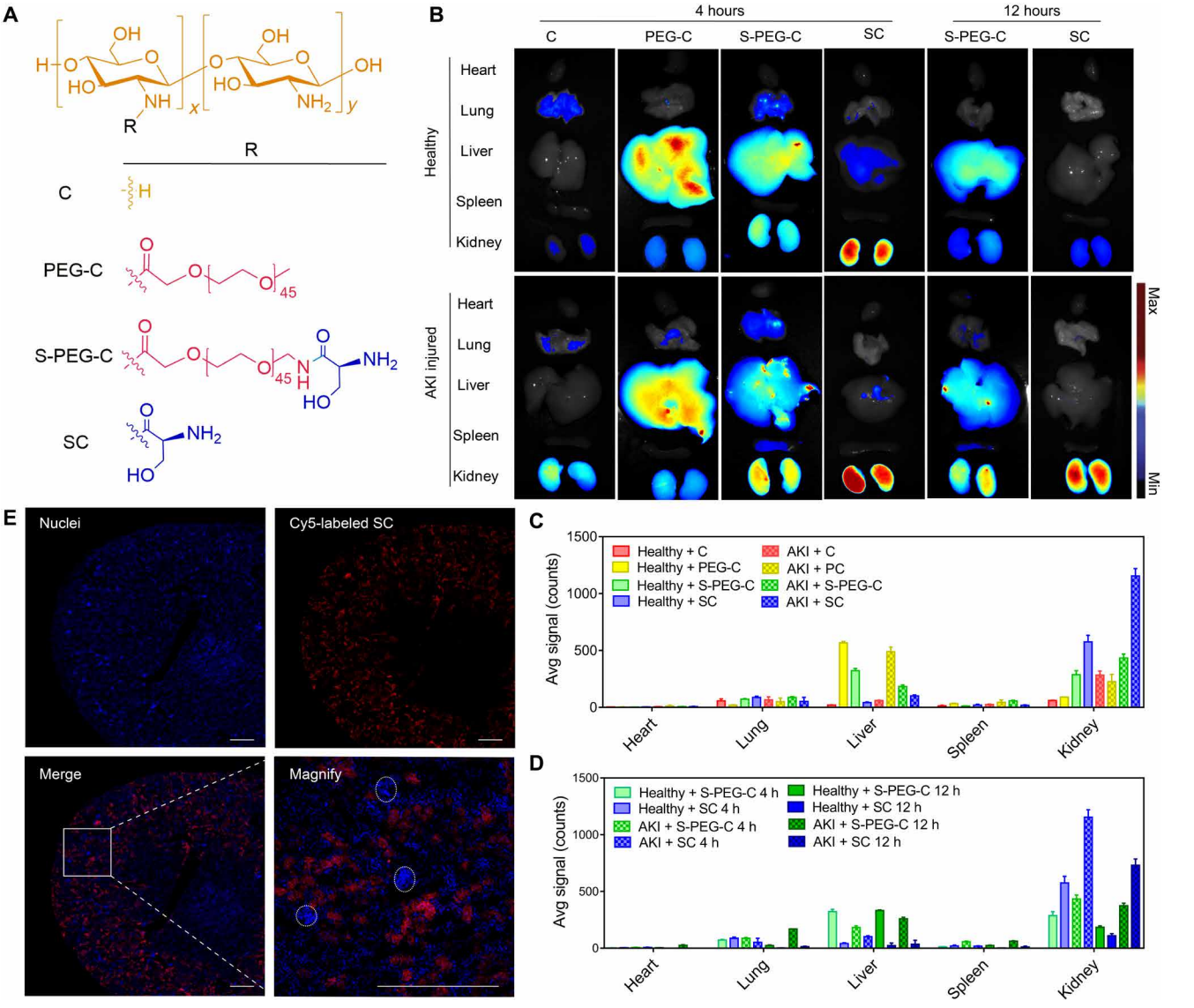

Fig. 2. Renal distribution and renal tubules accumulation of SC. (**A**) The chemical structures of SC and its analogies, C, PEG-C, and S-PEG-C. (**B**) Fluorescence images of the main organs (heart, lung, liver, spleen, and kidney) of mice at 4 or 12 hours after intravenous injection of Cy5-C, Cy5-PEG-C, Cy5-S-PEG-C, or Cy5-SC. One of three independent experiments is shown. Renal ischemia was induced by clamping of the bilateral renal pedicles for 30 min and then removed clamping to induce IR AKI. After the initiation of AKI, fluorescence-labeled SC and its analogies were administered intravenously. Four or 12 hours later, the main organs were harvested for fluorescence visualization. The healthy mice were treated with the same protocol as control. (**C** and **D**) Region of interest analysis of the kidney uptake at 4 and 12 hours after injection. The data are the means ± SD. $n = 3$ independent mice. (**E**) Representative confocal images of kidney sections after intravenous injection of Cy5-SC (red signal) for 4 hours. Blue indicates 4′,6-diamidino-2-phenylindole (DAPI) staining. White dashed circles denote glomeruli. Scale bars, 500 μm.

the other organs. In contrast, Cy5-SC mainly accumulated in the kidney at the same time point, showing much stronger florescence intensity than the other three carriers. In the case of AKI mice, the fluorescence intensity of the kidney in each group was increased to some extent as compared with normal mice. However, the fluorescence intensity of the Cy5-SC–treated kidney was increased much more than the other three groups. Those results demonstrated that SC had the best renal targeting ability than the other chitosan-based carriers. At 12 hours after injection, the fluorescent signals of Cy5-SC in the kidney were markedly decreased in normal mice. In contrast, most of the signals were retained in the kidney of AKI mice, indicating that SC could be rapidly cleared by the normal kidney but highly uptake by the AKI kidney (Fig. 2, B and D). For Cy5-S-PEG-C, the fluorescent signals in kidneys of normal and AKI mice were obviously decreased at 12 hours, and they were still widespread in livers and other organs. It was revealed that increasing the PEG modification is involved in the enhancement of shielding ability of formulations from destroy by enzyme or other physiological environment (*25*). We expect that this inexpensive and effective protection could prolong the circulation times and retention times of chitosan or SC, making prodrugs more resistant to denaturation and degradation. However, PEGylation of C or SC could change their physiochemical property, leading to a different biodistribution pattern and altering the kidney accumulation, limiting the drug delivery efficiency. Overall,

in vivo distribution study revealed that SC had the best renal targeting ability and longest retention time in the AKI kidney. Thus, SC was chosen as the optimal kidney–targeted carrier for the following study.

To investigate the renal tubular targeting ability of SC, we collected the renal sections of AKI mice at 4 hours after administration of Cy5-SC and then captured their microscopic fluorescence images. As depicted in Fig. 2E and fig. S4, the fluorescent signals of Cy5-SC in the kidney mainly located in the renal tubules [labeled by Lotus-tetragonolobus Lectin (LTL) in fig. S4], indicating the excellent renal tubular targeting ability of SC. The renal tubules are involved in the pathogenesis of kidney diseases, including AKI (*26*–*28*). The injury of renal tubules can induce tubular dysfunction and cell death in the forms of necrosis and apoptosis, therefore reduces renal functions (*29*). Thus, the high accumulation of SC in renal tubules indicates that SC is a potential drug carrier for effective AKI therapy.

Cellular uptake and Kim-1–targeted ability of SC

Before the evaluation of cellular internalization, in vitro cytotoxicity of SC toward human kidney 2 (HK-2) cells was performed by 3-(4,5-dimethylthiazol-2-yl)-2,5-diphenyltetrazolium bromide (MTT) assay. As shown in fig. S5, similar to chitosan, the viability of SC-treated cells was above 95% at a concentration up to 500 μg/ml, implying that SC was safe for biological application. The cellular internalization of Cy5-SC by HK-2 cells pretreated with or without H_2O_2 was then investigated by flow cytometry, in which Cy5-C was used as a control. As shown in Fig. 3A, after 2 hours of incubation with Cy5-SC, the fluorescence intensity of normal cells was nonsignificantly different from that of injured cells. Similar result was observed in Cy5-C–treated cells. On the other hand, the injured cells showed a much higher fluorescence intensity than normal cells when they were incubated with Cy5-SC for 6 hours. In comparison, normal and injured cells treated with Cy5-C still had a similar

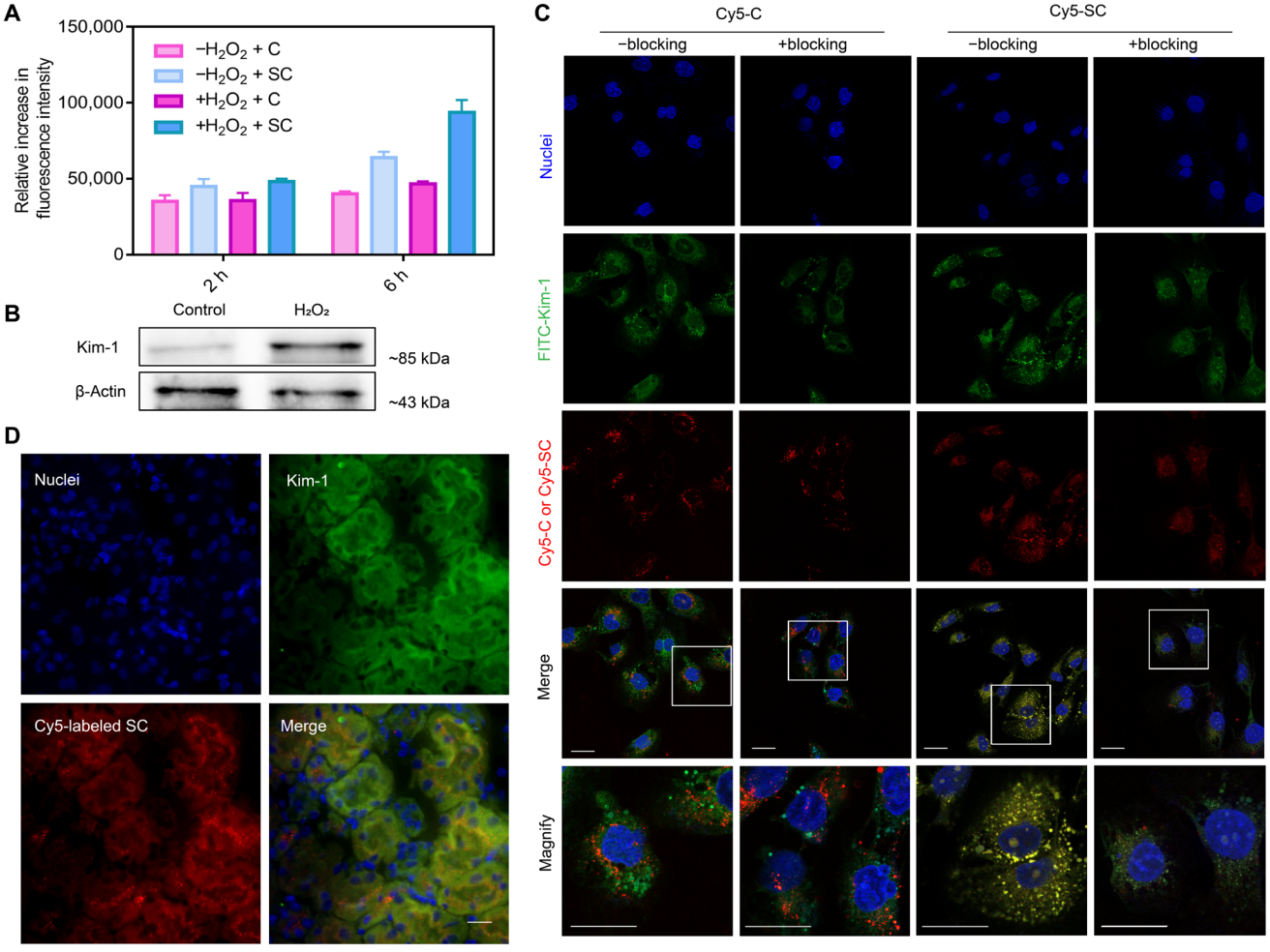

Fig. 3. Kim-1–associated endocytosis of SC in vitro and in vivo. (**A**) Flow cytometry assay of cellular uptake of Cy5-C and Cy5-SC in normal or H_2O_2-stimulated HK-2 cells for 2 or 6 hours. The data are the means ± SD. $n = 3$. (**B**) Western blotting analysis of Kim-1 expression using lysates from normal and H_2O_2-stimulated HK-2 cells. (**C**) Representative confocal images of HK-2 cells that were previously stimulated with H_2O_2 at a concentration of 500 μM for 4 hours and then treated with Cy5-C and Cy5-SC for another 4 hours (red signal). "+Blocking" indicates pretreatment with Kim-1 antibody at a concentration of 30 μg/ml for 0.5 hours before administration of Cy5-C or Cy5-SC. "−Blocking" indicates without treatment of Kim-1 antibody. Experiments were repeated three times. Nuclei, staining with DAPI, are shown in blue. Green indicates immunostaining for Kim-1. The bottom images correspond to magnified views of the boxed areas above. Scale bars, 20 μm. FITC, fluorescein isothiocyanate. (**D**) Representative confocal images of kidney sections from AKI-injured mice after intravenous injection of Cy5-SC (red signal) for 4 hours. Blue indicates DAPI staining. Immunostaining for Kim-1 is shown in green. Scale bar, 20 μm.

fluorescence intensity after 6 hours of incubation. The results agreed well with the results of in vivo distribution in Fig. 2B.

Kim-1 is a transmembrane protein that is markedly up-regulated in the kidney of renal diseases, particularly in the injured proximal tubules (*22*). Western blot results obtained in our study also suggested that H_2O_2 stimulation considerably up-regulated the levels of Kim-1 in HK-2 cells (Fig. 3B). We hypothesized that the higher cellular uptake of SC by H_2O_2-stimulated cells was associated with the specific interaction between Kim-1 and SC. To prove our hypothesis, we performed colocalization between SC and Kim-1 by confocal laser scanning microscopy (CLSM; Fig. 3C). The H_2O_2-stimulated cells pretreated with or without the blocking agent of Kim-1 antibody were incubated with Cy5-C or Cy5-SC for 6 hours. Fluorescence images revealed that Kim-1 was present on the surface of H_2O_2-stimulated cells. In the absence of Kim-1 antibody, the cells treated with Cy5-SC had a stronger colocalized signals (Cy5-SC and Kim-1) than that of Cy5-C–treated ones (Cy5-C and Kim-1), demonstrating the specific binding between SC and Kim-1. In the presence of Kim-1 antibody, the cellular internalization of Cy5-SC was slowed down, showing a decreased fluorescent signal in the cells. Thus, less colocalization between Cy5-C and Kim-1 was observed. In comparison, the presence of Kim-1 antibody had little impacts on the cellular uptake of Cy5-C. These findings further confirmed that the up-regulation of Kim-1 in the injured renal cells facilitated the cellular internalization of SC via the specific interaction between Kim-1 and SC. The renal sections of AKI mice were collected at 4 hours after administration of Cy5-SC, and their microscopic fluorescence images were then captured as shown in Fig. 3D. Consistent with the result in Fig. 3C, well colocalization of Kim-1 and Cy5-SC was observed.

Synthesis and characteristics of SS31 prodrugs

In this section, three types of SS31-based prodrugs were synthesized, including ROS-sensitive prodrugs of SC-TK-SS31, C-TK-SS31, and ROS-insensitive prodrug of SC–nonane diacid(NO)–SS31 (fig. S1).The successful conjugation of SS31 onto the backbones of SC or C via TK or nonane diacid (NO) linker was confirmed by the appearance of peaks at ~6.4 ppm (attributed to the protons of aromatic ring in SS31), peaks at ~2.4 and ~ 2.6 ppm (attributed to methylene groups in TK), or peaks at ~2.1 ppm (attributed to methylene groups in NO) in the SC-TK-SS31, C-TK-SS31, or SC-NO-SS31 spectra, as shown in fig. S2. The substitution ratio of SS31 of SC-TK-SS31, C-TK-SS31, or SC-NO-SS31 was calculated to be around 1/1 (SS31/C, mol/mol). The SS31 contents measured by high-performance liquid chromatography (HPLC) in SC-TK-SS31 and C-TK-SS31 were approximately 16.8 and 19.6%, respectively, which were agreed well with the theoretical values calculated from substitution ratio. The molecular weight of SC-TK-SS31 was further measured by GPC, as 3.78 kDa (fig. S3). The substitution ratio of SS31 of SC-TK-SS31 was calculated according to the GPC results to be 1/1 (SS31/C, mol/mol), which was coincident with the results mentioned above.

We further investigated the stability of SC-TK-SS31 in plasma (fig. S6). SC-TK-SS31 was incubated with plasmas of mice at a concentration of SS31 (10 μg/ml) in a 37°C incubator for 24 hours, in with SS31 that was used as control. More SS31 was preserved in the plasmas incubated with SC-TK-SS31 relative to that incubated with SS31 (SC-TK-SS31 versus SS31, 91.9 ± 3.2% versus 81.1 ± 3.6%), which indicated that SC-TK-SS31 had plasma stability. For our formulation, L-serine modification slightly weakened the cationic property of chitosan, which might improve the plasma stability of SC-TK-SS31.

ROS-responsive cleavage and mitochondria-targeted ability of SC-TK-SS31

The TK linker in SC-TK-SS31 is expected to be cleaved by ROS, thereby achieving an on-demand drug release. H_2O_2 as a typical and relatively stable ROS stimulator was used to investigate the ROS responsibility of SC-TK-SS31, where the ROS-insensitive prodrug of SC-NO-SS31 was used as a control. HPLC was used to monitor the cleavage of TK and release of SS31 from SC-TK-SS31 in the presence of 10 mM H_2O_2. As shown in Fig. 4A, SC-TK-SS31 exhibited a peak at an elution time of 3.4 min. Along with time, the peak at elution time of 3.4 min decreased gradually. When SC-TK-SS31 exposing at a H_2O_2 concentration of 10 mM, a new peak at elution time of 4.1 min appeared within 2 hours and increased gradually. The HPLC trace of pure SS31 suggested the peak at an elution time of 4.1 min belonged to SS31 (fig. S7A). We further evaluated the component with an elution time of 4.1 min by HPLC–mass spectrometry (HPLC-MS) (fig. S7B). The abundant ions at a mass/charge ratio of 640.3934 and 320.7007 stood for the singly protonated, singly charged ion $[SS31 + H]^+$ and the doubly protonated, doubly charged ion $[SS31 + 2H]^{2+}$, respectively. Therefore, the mass spectrum could demonstrate that the released component with an elution time of 4.1 min was mainly pure SS31 and the release of active pure SS31 was meaningful and crucial for the good therapeutic efficiency of SC-TK-SS31. The decrease in peak at an elution time of 3.4 min was not fast owing to the disturbance of ultraviolet (UV) absorbance of chitosan at a wavelength of 220 nm, as shown in fig. S7C. Therefore, we evaluated the release profile of SS31 in SC-TK-SS31 mainly according to the peak area at an elution time of 4.1 min. The released SS31 increased along with time as shown in Fig. 4 (A and B). Around 60% of SS31 was released from SC-TK-SS31 at initial 8 hours, after which the drug release rate slowly reduced until a relatively stable value of ~80% was reached more than 48 hours, which was attributed to cleavage of TK linker illustrated in Fig. 4C. As shown above, SS31 will be released ultimately in the degradation process. In contrast, the sign of SS31 release was not observed in SC-NO-SS31 exposing at a H_2O_2 concentration of 10 mM, indicating that SC-NO-SS31 was highly insensitive to H_2O_2. The results were further confirmed by cellular fluorescence colocalization study.

The ROS-responsive SS31 release of SC-TK-SS31 in H_2O_2-stimulated cells was investigated by CLSM. For visible observation of SS31 release behavior, Cy5-SC-TK-SS19 was synthesized in this part, where SS19 was used as a fluorescent analog of SS31 (*30*). The cells treated with or without H_2O_2 were incubated with Cy5-SC-TK-SS19 for a predetermined time (4 and 12 hours), and Cy5-SC-NO-SS19 was applied as a control. As shown in Fig. 4 (E and F), the fluorescent signal of SS19 (blue color) was well overlapped with that of Cy5-SC (red color) when the H_2O_2-stimulated cells were incubated with Cy5-SC-TK-SS19 for 4 hours. However, the overlapping signals of SS19 and Cy5-SC in H_2O_2-stimulated cells became less at 12 hours, suggesting that SS19 was released from Cy5-SC-TK-SS19 at a prolonged time on the basis of enhanced ROS concentration inside injured cells. By contrast, obvious separation of blue and red fluorescence was not observed in normal cells at 4 or 12 hours, suggesting that Cy5-SC-TK-SS19 was stable in the absence of H_2O_2. Similarly, Cy5-SC-NO-SS19 was also stable without the separation of overlapping

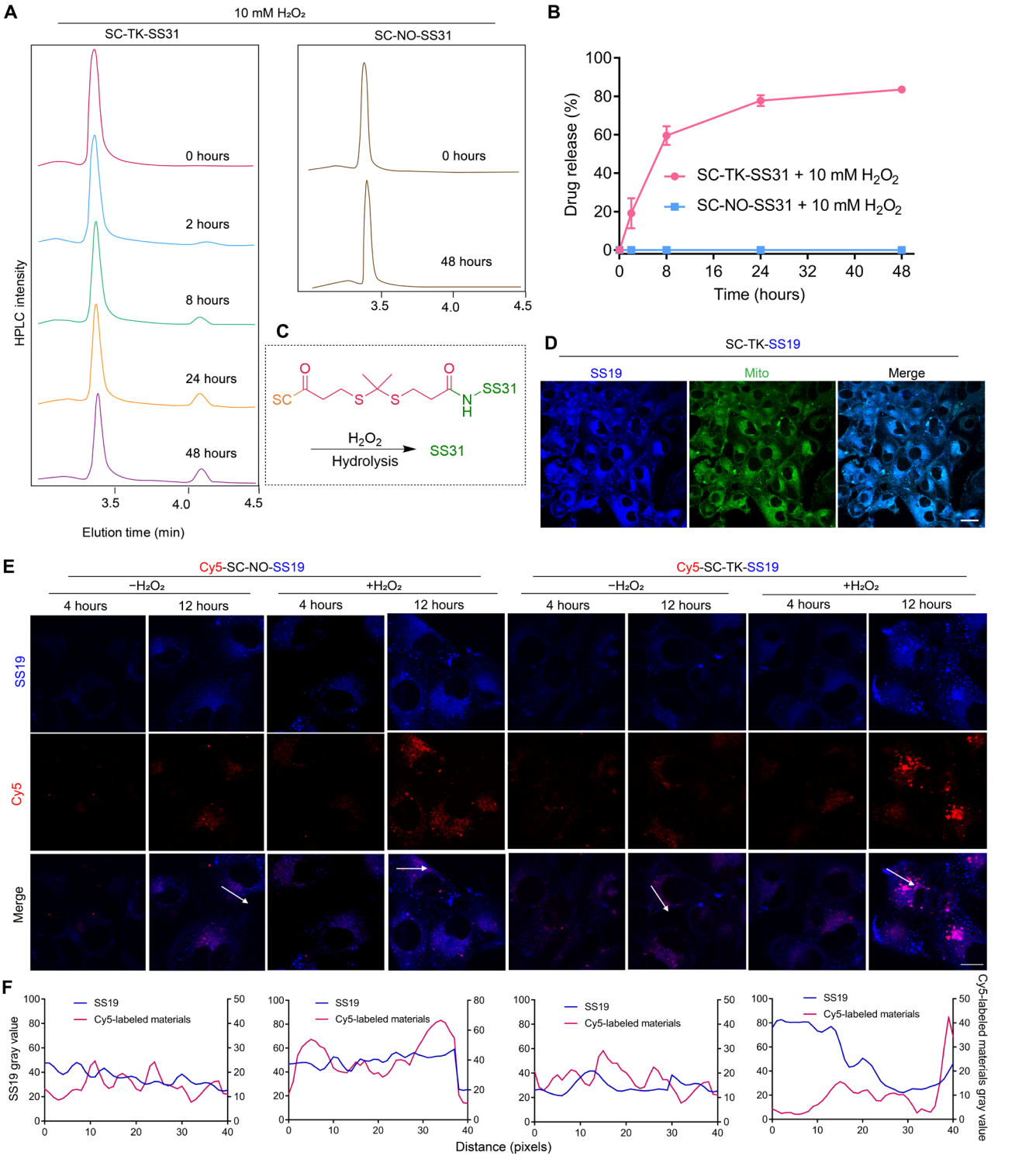

Fig. 4. H_2O_2-triggered cleavage of SC-TK-SS31 and ROS-sensitive drug release inside the H_2O_2-stimulated HK-2 cells. (**A**) Absorption peaks of SC-TK-SS31 in the presence of 10 mM H_2O_2 monitored by HPLC at a wavelength of 220 nm. SC-NO-SS31 (irresponsive prodrug) was treated as control. Peaks with an elution time of 4.1 min represent SS31. (**B**) The release profiles of SC-TK-SS31 and SC-NO-SS31 in the presence of 10 mM H_2O_2 monitored by HPLC. The data are the means ± SD. $n = 3$. (**C**) Schematic illustration of TK cleavage. (**D**) Representative confocal images of H_2O_2-stimulated HK-2 cells after incubated with SC-TK-SS19 for 12 hours. Blue indicates SS19, representing SS31. MitoTracker-stained mitochondria are shown in green. Scale bar, 40 μm. (**E**) Representative confocal images of colocalization of SS19 (the fluorescent analog of SS31, representing drug, blue signal) with Cy5-SC (representing carriers, red signal). Cy5-SC-NO-SS19 was treated as control. The white arrows denote the left side to right side of the intensity profiles in (F). Scale bar, 10 μm. (**F**) The level of overlay of SS19 and Cy5-labeled carriers.

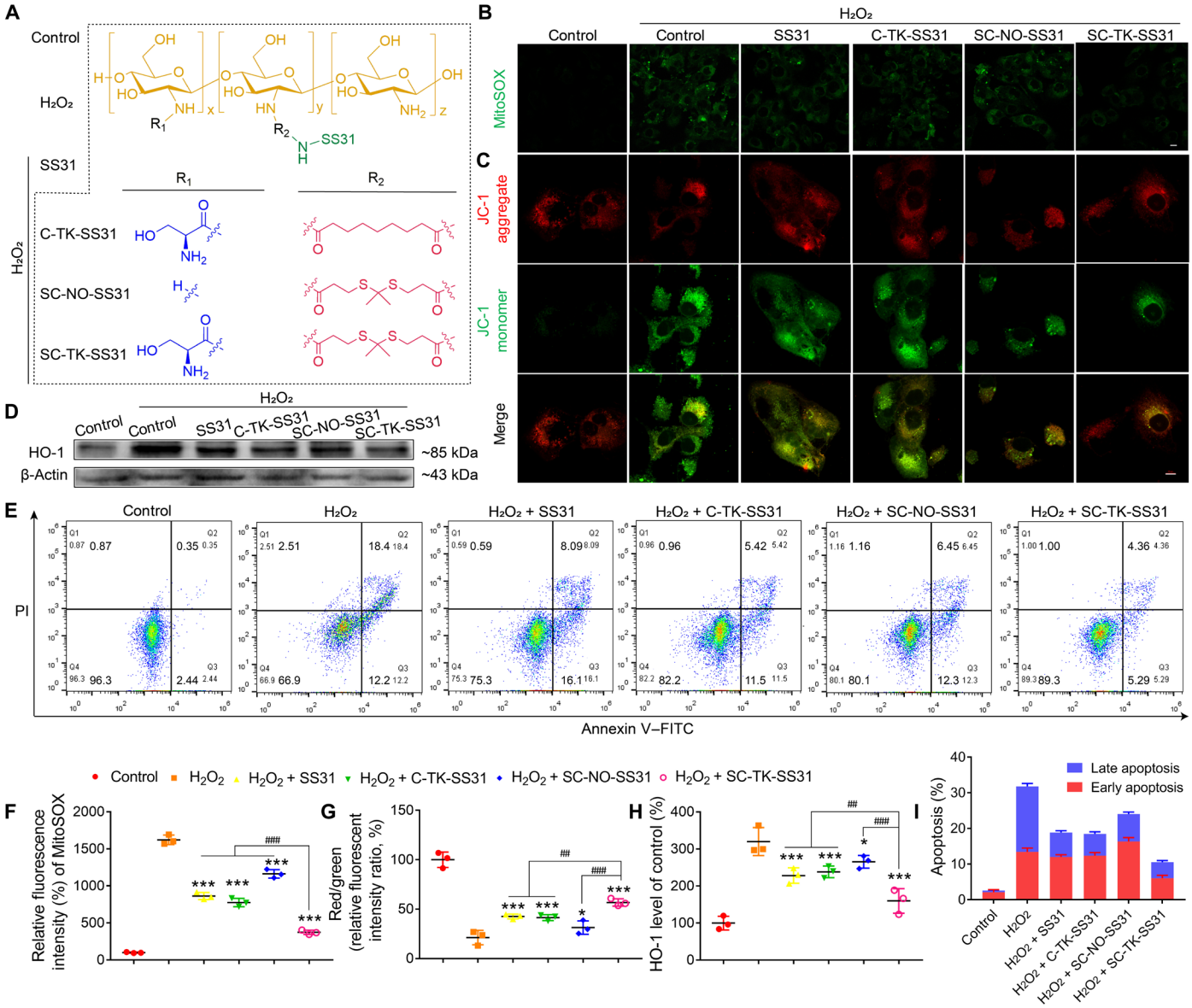

Fig. 5. Relief of oxidative stress and apoptosis by SC-TK-SS31 in vitro. H_2O_2-stimulated HK-2 cells were treated with SS31, C-TK-SS31, SC-TK-SS31, or SC-NO-SS31 at an SS31 concentration of 20 μg/ml for 24 hours. (**A**) The experimental groups for evaluating therapeutic effect of SC-TK-SS31, pure SS31, and the analogies of SC-TK-SS31 including C-TK-SS31 and SC-NO-SS31. The chemical structures of SC-TK-SS31 and its analogies, C-TK-SS31 and SC-NO-SS31. (**B**) Fluorescence images of mitochondrial ROS analysis with MitoSOX in H_2O_2-stimulated cells after different treatments. Scale bar, 20 μm. (**C**) Fluorescence images of JC-1 assay to measure mitochondrial membrane depolarization in H_2O_2-stimulated cells after different treatments. Scale bar, 10 μm. (**D**) Western blotting analysis of HO-1 expression in H_2O_2-stimulated HK-2 cells after different treatments. (**E**) Flow cytometry–based apoptosis assay by the Annexin V–FITC Apoptosis Kit. PI, propidium iodide. (**F**) The MitoSOX mean fluorescence intensity of (B). (**G**) The mean ratio of fluorescence intensity of JC-1 aggregates and JC-1 monomers in (C). (**H**) Densitometric analysis of Western blotting of HO-1 expression in (D). (**I**) The mean percentage of apoptotic cells in (E). $n = 3$, $^*P < 0.05$ and $^{***}P < 0.001$ as compared with H_2O_2 group. $n = 3$, $\#\#P < 0.01$ and $\#\#\#P < 0.001$ between groups as indicated.

signals being observed, regardless of whether H_2O_2 was present. These results further confirmed that SC-TK-SS31 had a relatively high ROS responsibility. In addition, the cellular uptake of free SS19 was also tested. As shown in fig. S8, the fluorescence intensity of SS19-treated normal or injured HK-2 cells was unobviously different, suggesting that SS19 had no cellular selectivity. In contrast, as shown in Fig. 4E, the fluorescence intensity of Cy5-SC-TK-SS19 in H_2O_2-stimulated cells was significantly higher than that in normal cells, which was coincident with flow cytometry assay of Cy5-SC in Fig. 3A.

As mentioned earlier, SS31 is a mitochondria-targeted antioxidant that can be used for the treatment of AKI. Mitochondria-targeted ability of SS31 was also verified in fig. S9. To investigate the mitochondria-targeted ability of SC-TK-SS31, we treated H_2O_2-stimulated cells with SC-TK-SS19 for 12 hours, followed by CLSM observation. The CLSM images showed that the blue fluorescence (SS19) evidently overlapped with the green fluorescence (MitoTracker Green) inside the cells (Fig. 4D). The result suggested that SS31 carried by SC-TK-SS31 could accumulate in the mitochondria, which was the premise for SS31 to relief AKI.

Antioxidative stress and antiapoptosis of SC-TK-SS31 in vitro

In this part, the influence of formulation types on in vitro antioxidative stress and antiapoptotic efficiencies was investigated (Fig. 5). The structure of SS31 prodrugs and experimental groups was illustrated in Fig. 5A. First, the ability of SS31, C-TK-SS31, SC-NO-SS31, and SC-TK-SS31 to reduce mitochondrial ROS production in HK-2 cells was investigated by CLSM via a mitochondrial ROS probe (MitoSOX). It was observed that the fluorescence intensity of ROS probe was largely enhanced by stimulating the cells with H_2O_2 (Fig. 5, B and F). This result demonstrated that the ROS level in the cells was considerably increased in the presence of H_2O_2. The treatment of SC-TK-SS31 caused a marked decrease in the fluorescence intensity, which was lower than those treated with SS31, C-TK-SS31, or SC-NO-SS31. This observation indicated that SC-TK-SS31 had the best ability to reduce mitochondrial ROS production than the other three drugs. Next, the effect of formulation types on oxidative stress was investigated by evaluating the change in the expression level of heme oxygenase-1 (HO-1) protein, which is an antioxidative enzyme that could be remarkably up-regulated under high ROS levels (*31*). As expected, the expression level of HO-1 was largely increased when the cells were treated with H_2O_2 (Fig. 5, D and H). After the H_2O_2-treated cells were incubated with SC-TK-SS31, SS31, C-TK-SS31, or SC-NO-SS31, the expression level of HO-1 was significantly decreased. However, the expression level of HO-1 in SC-TK-SS31–treated cells was much lower than the other three groups, further confirming the best antioxidative ability of SC-TK-SS31. After that, JC-1 (5′,6,6′-tetrachloro-1,1′,3,3′-tetraethylbenzimidazolylcarbocyanine iodide) dye was exploited to investigate the changes in mitochondrial membrane potential (MMP). As shown in Fig. 5 (C and G), the red/green fluorescence intensity ratio was decreased obviously after the cells were incubated with H_2O_2 for 24 hours, demonstrating that the H_2O_2-induced oxidative stress greatly lowered the MMP of HK-2 cells. The red/green fluorescence intensity ratio in H_2O_2-treated cells was significantly enhanced after the treatment of SS31, C-TK-SS31, or SC-NO-SS31. As compared with SS31, C-TK-SS31, and SC-NO-SS31, the treatment of SC-TK-SS31 could cause a larger enhancement of red/green fluorescence intensity ratio, revealing the strongest ability of SC-TK-SS31 to stabilize the MMP by relieving the oxidative stress in the mitochondria.

It is well known that mitochondria play a vital role on the regulation of cell apoptosis (*10*). Thus, the effect of formulation types on the cell apoptosis was examined using flow cytometry (FCM). As shown in Fig. 5 (E and I), compared with control groups, H_2O_2-treated HK-2 cells demonstrated a markedly increased apoptosis rate. The treatment of SS31, C-TK-SS31, and SC-NO-SS31 significantly decreased the cell apoptosis caused by H_2O_2 stimulation. In comparison, SC-TK-SS31 revealed a larger reduction of cell apoptosis in H_2O_2-treated cells, indicating that SC-TK-SS31 has the most powerful capability in protecting cell apoptosis from oxidative stress.

Treatment of AKI

The ability of SC-TK-SS31 to alleviate AKI was investigated using IR-induced AKI mouse model. After AKI modeling, the SC-TK-SS31, SS31, C-TK-SS31, and SC-NO-SS31 were administrated by intravenous injection, followed by collecting the serum and kidneys 48 hours later for further evaluation (see Fig. 6A and Materials and Methods). High levels of serum creatinine and blood urea nitrogen (BUN) are

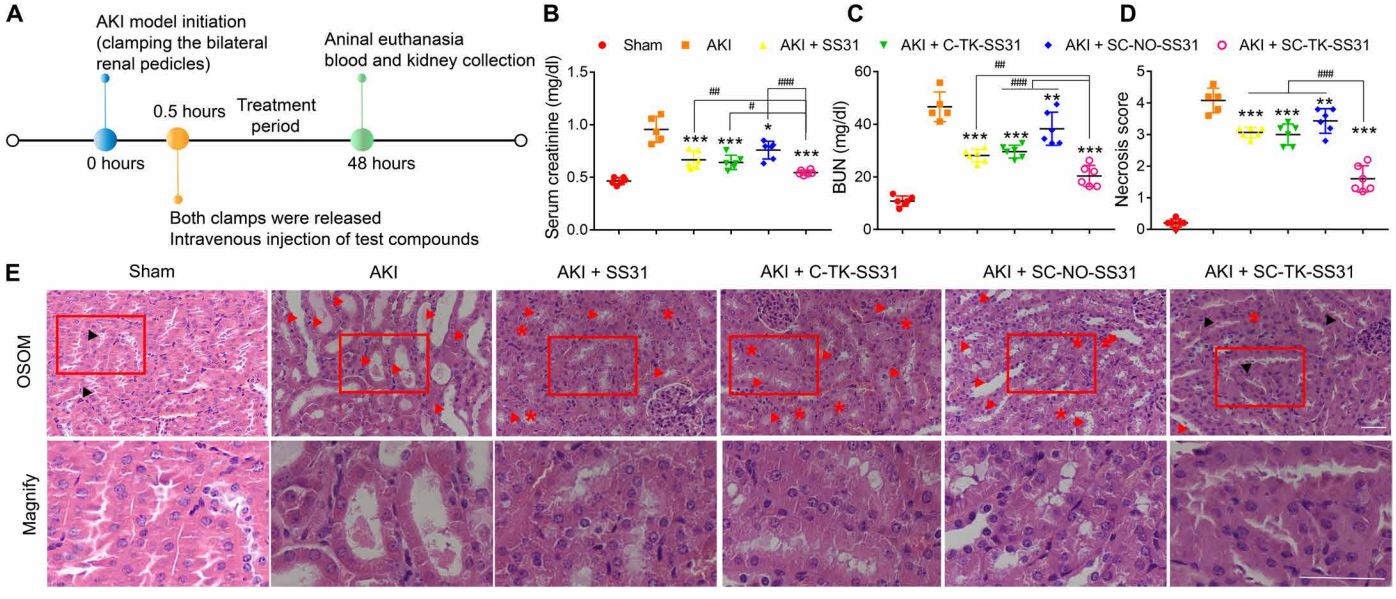

Fig. 6. Amelioration of renal functions by SC-TK-SS31 in vivo. (**A**) After initiation of IR-induced AKI, different agents (SS31, C-TK-SS31, SC-NO-SS31, and SC-TK-SS31) were administered intravenously at an SS31 dosage of 2 mg/kg. Forty-eight hours later, blood and kidneys were collected for evaluation. (**B** and **C**) Serum analysis of creatinine and BUN in AKI mice after different treatments. (**D**) Cell necrosis score in outer stripe of the outer medulla (OSOM) of AKI mice after different treatments. (**E**) H&E staining of kidney tissues in the OSOM. Scale bar, 50 μm. Kidneys of sham-operated mice represented normal architecture with remarkable brush borders (shown as black arrowheads) in tubules. Serious necrosis was observed in kidneys of saline-treated mice. Red arrowheads donate hyaline casts and cell sloughing. Asterisks donate adhesion. Focal necrosis was indicated in SS31-, C-TK-SS31–, and SC-NO-SS31–treated groups. Cell sloughing and adhesion can be observed. Necrosis was rare in the SC-TK-SS31–treated mice with brush borders presented in tubules. The bottom images correspond to magnified views of the boxed areas above. Scale bar, 50 μm. All data are expressed as means ± SD. $n = 5$ and 6 in each group, $^*P < 0.05$, $^{**}P < 0.01$, and $^{***}P < 0.001$ as compared with saline. $n = 5$ and 6 in each group, $\#P < 0.05$, $\#\#P < 0.01$, and $\#\#\#P < 0.001$ between groups as indicated. n.s., no significant difference.

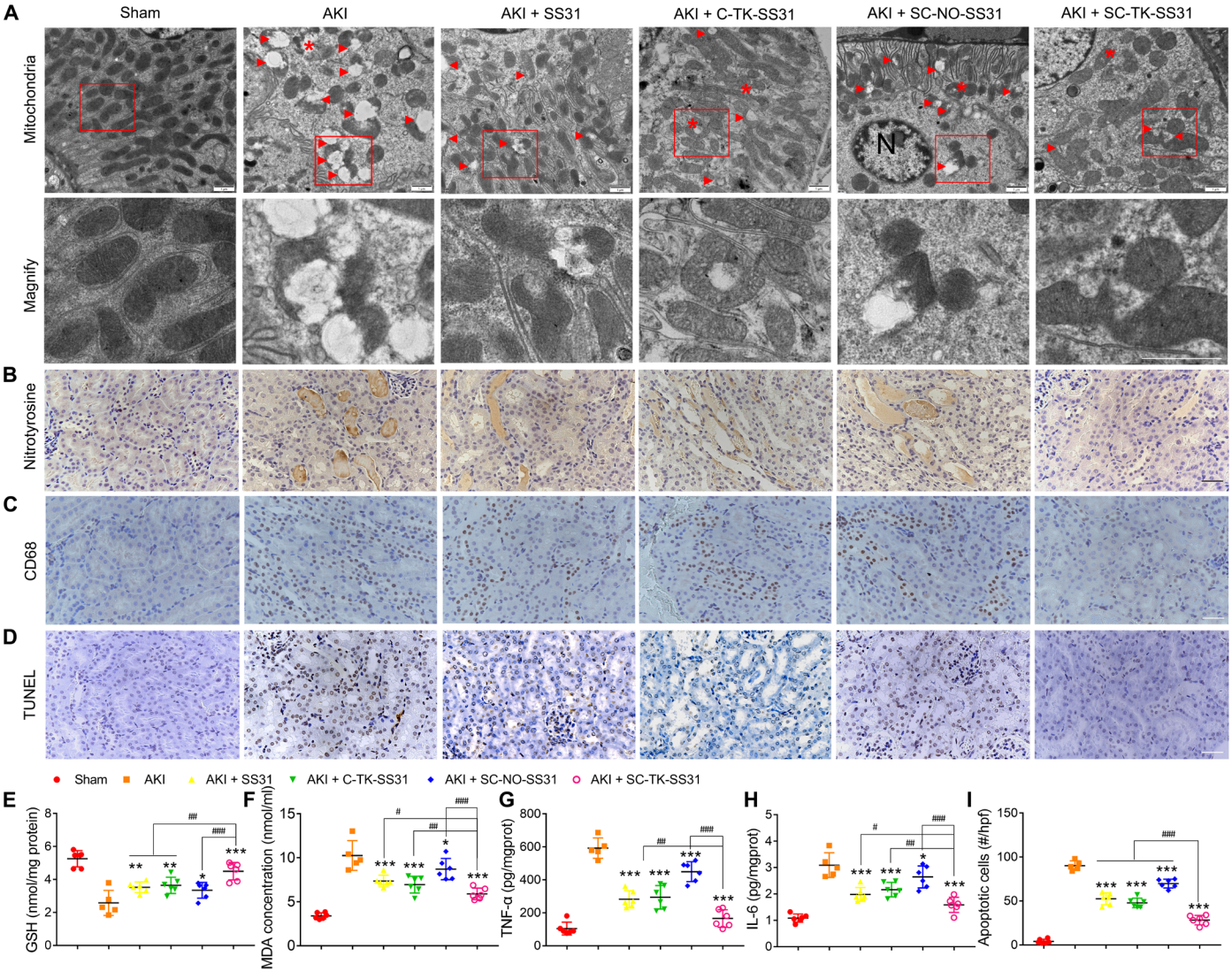

Fig. 7. SC-TK-SS31–protected mitochondria from damage and reduced the oxidative stress, inflammation, and apoptosis in AKI mice. (**A**) Bio-TEM image of mitochondria in outer medulla. Swollen mitochondria with disrupted cristae architecture are noted with arrowheads. Mitochondria with disruption of membranes and release of matrix materials into the cytosol are noted with arrowheads. N, nucleus. Scale bar, 1 μm. (**B**) Immunohistochemical staining (brown) with nitrotyrosine, a marker of peroxidation. Scale bar, 50 μm. (**C**) Macrophage immunostaining using anti-CD68 antibody. Scale bar, 50 μm. (**D**) Terminal deoxynucleotidyl transferase–mediated deoxyuridine triphosphate nick end labeling (TUNEL) assay for apoptosis cells staining (brown nuclei) in outer medulla in AKI mice with different treatments. Scale bar, 50 μm. (**E** and **F**) GSH and MDA level changes in AKI mice after different treatments. (**G** and **H**) Renal cytokine TNF-α and IL-6 alternation in AKI mice after different treatments. (**I**) The number of TUNEL$^+$ cells per high-power field (hpf) in the sham or AKI group with different treatments. All data are expressed as means ± SD. $n = 5$ and 6 in each group, $^*P < 0.05$, $^{**}P < 0.01$, and $^{***}P < 0.001$ as compared with saline. $n = 5$ and 6 in each group, $\#P < 0.05$, $\#\#P < 0.01$, and $\#\#\#P < 0.001$ between groups as indicated.

effective clinical indices of the damaged kidney function (*32*, *33*). As indicated in Fig. 6 (B and C), the treatment of SS31, C-TK-SS31, and SC-NO-SS31 lowered the levels of creatinine and BUN in AKI mice. However, obviously lower levels of creatinine and BUN were detected for SC-TK-SS31 treatment group, indicating that SC-TK-SS31 could effectively restore renal function in the AKI mice. We further analyzed hematoxylin and eosin (H&E) staining kidney sections from each group (Fig. 6, D and E). Normal renal architecture was shown in the sham group, as evidenced by brush borders in the proximal tubules. Necrosis was observed in the AKI group that hyaline casts and sloughed cells filled many tubules. Focal necrosis was observed in SS31-, C-TK-SS31–, and SC-NO-SS31–treated groups, while the SC-TK-SS31 treatment group reduced damage more considerably and the brush borders were well preserved in proximal tubules.

Transmission electron microscopy (TEM) images of renal tissue revealed that AKI resulted in extensive damage to mitochondria in proximal tubular cells, as reflected by the fact that many swollen mitochondria with loss of cristae were observed and some mitochondria showed disrupted membranes and release of matrix material into the cytoplasm (Fig. 7A). The treatment of SS31, C-TK-SS31, and SC-NO-SS31 largely decreased the numbers of damaged mitochondria in proximal tubular cells of AKI mice. In comparison, samples from SC-TK-SS31–treated AKI mice showed less numbers

of damaged mitochondria, with many elongated mitochondria with preservation of cristae structure being observed.

To evaluate antioxidative stress effect of SC-TK-SS31 in the kidney of AKI, we performed immunohistochemical staining of nitrotyrosine. Nitrotyrosine is formed on protein tyrosine residues by peroxynitrite-induced nitration and is considered a sensitive marker for oxidative stress (Fig. 7B) (*34*). The numbers of nitrotyrosine-positive tubules significantly increased in AKI mice. SS31, C-TK-SS31, and SC-NO-SS31 treatment decreased the numbers of nitrotyrosine-positive tubules in AKI mice. However, SC-TK-SS31 revealed more obvious reduction of nitrotyrosine caused by AKI. Staining of nitrotyrosine was negative in sham mice without AKI. The levels of glutathione (GSH), intracellular neutralizer of ROS (*35*), and malondialdehyde (MDA), indicator of the extent of injure caused by ROS (*36*), in kidney tissue were also investigated (Fig. 7, E and F). There was significant depletion of GSH detected in AKI kidney tissues. SS31, C-TK-SS31, and SC-NO-SS31 treatment alleviated the depletion of GSH; however, higher GSH level was detected in SC-TK-SS31 group. Increased levels of MDA were found in the AKI mice. SS31, C-TK-SS31, and SC-NO-SS31 treatment decreased the levels of MDA of AKI-modeled mice, while lower MDA levels were found in SC-TK-SS31 group.

Macrophages migrating to the AKI kidney represent apoptotic cell death (*37*). As shown in Fig. 7C, there was an obvious increase in macrophages that was in the kidney of AKI group. The treatment of SS31, C-TK-SS31, and SC-NO-SS31 reduced the AKI-induced macrophages infiltration, whereas fewer macrophages were observed in SC-TK-SS31–treated group. We further measured the levels of proinflammatory cytokines in the kidney tissues, including interleukin-6 (IL-6) and tumor necrosis factor–α (TNF-α). As shown in Fig. 7 (G and H), the levels of IL-6 and TNF-α were significantly elevated in the AKI group. In comparison, the treatment of SC-TK-SS31, SS31, C-TK-SS31, and SC-NO-SS31 led to a decrease in the expression levels of IL-6 and TNF-α. Among the treatment groups, SC-TK-SS31 had the lowest cytokines levels, suggesting that SC-TK-SS31 had the strongest anti-inflammatory capability.

AKI-induced oxidative stress often leads to apoptotic cell death (*9*). Terminal deoxynucleotidyl transferase–mediated deoxyuridine triphosphate nick end labeling (TUNEL) assay was performed to measure the apoptotic cells in the AKI-injured kidney. Apoptotic cells in SS31, C-TK-SS31, and SC-NO-SS31 groups were obviously decreased when compared with AKI group. SC-TK-SS31 group still showed the lowest numbers of apoptotic cells, indicating the best antiapoptotic effect of SC-TK-SS31 (Fig. 7, D and I).

The concentrations of SS31 in main organs

We determined the concentrations of SS31 in main organs (kidney, heart, lung, liver, and spleen) of AKI mice for further detecting the AKI kidney–targeted ability of SC-TK-SS31. At 4 hours after injection in a SS31 dose of 2 mg/kg, more drugs were determined in kidneys of SC-TK-SS31 group relative to that of SS31 group and C-TK-SS31 group (SC-TK-SS31, 2.23 ± 0.12 μg/g; SS31, 0.74 ± 0.04 μg/g; C-TK-SS31, 1.08 ± 0.20 μg/g), which was coincident with the fluorescent results in Fig. 2B. It was further confirmed that SC-TK-SS31 had the superiority as an AKI kidney–targeted prodrug (fig. S10).

DISCUSSION

In the study, we synthesized AKI kidney–targeted chitosan-based drug carrier, SC, which can rapidly and effectively accumulate in the AKI kidney, especially in renal tubules. We found that the modification of PEG (the widely used carrier material for various diseases including renal diseases) altered the renal accumulation, shown as the high uptake in other organs except for kidneys. In addition, SC can effectively retain in the kidney of AKI mice rather than be rapidly eliminated, which is essential for enhanced therapeutic effect. The renal accumulation and retention of SC in AKI kidneys is attributed to the preferential internalization by injured renal tubular cells through Kim-1–mediated endocytosis. Kim-1 received much attention in early diagnosis and pathological mechanisms of kidney diseases (*38*, *39*). However, it is a new field for Kim-1 as a drug target.

Conjugating SS31, a mitochondria-targeted antioxidant, to SC via ROS-sensitive TK linker, the precisely stepwise-targeted prodrug (SC-TK-SS31) was synthesized. SC-TK-SS31 accumulated in the AKI kidney (organ), retained in renal tubules (tissue), internalized by injured tubular cells (cell), responsively release SS31, which further targeted to mitochondria (organelle) to relief mitochondrial damage and further alleviate AKI. On the basis of precise accumulation and sensitive release, SC-TK-SS31 significantly enhanced the therapeutic effect of SS31. The excellent biocompatibility and rapid therapeutic response in AKI mice suggested that SC-TK-SS31 is a promising candidate for the treatment of clinical AKI. The precisely stepwise targeting delivery strategy can also be applied for the treatment of other kidney disease, such as renal cancer.

MATERIALS AND METHODS

Materials

Chitosan (C; molecular weight, ~2.5 kDa) was purchased from Qingdao BZ Oligo Biotech Co. Ltd. (Qingdao, China). Boc-L-Ser(tBu)-OH and SS31 were purchased from Popchem Co. Ltd. (Hefei, China). NH_2-PEG-COOH (molecular weight, ~2 kDa) and mPEG-COOH (molecular weight, ~2 kDa) were purchased from ToYongBio Co. Ltd. (Shanghai, China). *O*-(*N*-succinimidyl)-*N*,*N*,*N*′,*N*′-tetramethyluronium tetrafluoroborate (TSTU), TFA, and triisopropylsilane (TIS) were purchased from Aladdin Co. Ltd. (Shanghai, China). Nonane diacid and *p*-toluenesulfonic acid (TsOH) were purchased from Macklin Co. Ltd. (Shanghai, China). Cy5–*N*-hydroxysuccinimide (NHS) was purchased from Dalian Meilun Biotechnology Co. Ltd. (Dalian, China). MTT were purchased from Sigma-Aldrich (St. Louis, MO, USA). 2-(4-Amidinophenyl)-1*H*-indole-6-carboxamidine [4′,6-diamidino-2-phenylindole (DAPI)], bicinchoninic acid (BCA) protein assay kit, anti–HO-1 antibody, and the secondary anti-rabbit immunoglobulin G (IgG) horseradish peroxidase (HRP) were purchased from Beyotime Biotechnology Co. Ltd. (Shanghai, China). β-Actin antibodies were purchased from Boster Biological Technology Co. Ltd. Nitrotyrosine antibodies were purchased from GeneTex. SS19 was purchased from ChinaPeptides (Shanghai, China). The commercial enzyme-linked immunosorbent assay (ELISA) kits of TNF-α and IL-6 were obtained from Jiangsu Feiya Biological Technology Co. Ltd. (Jiangsu, China). Superoxide dismutase (SOD) and MDA kits were purchased from Nanjing Jiancheng Bioengineering Institute, Nanjing, China. A TUNEL assay kit was obtained from Roche (Nutley, NJ, USA). Fluorescein-labeled LTL (#FL-1321) were purchased from Vector Laboratories (USA). All other solvents were of analytical or chromatographic grade.

Synthesis and characteristics of chitosan-based carrier materials

To synthesize L-serine–modified chitosan (SC), chitosan was reacted with Boc-Ser(tBu)-OH using TSTU method. A solution of

Boc-Ser(tBu)-OH (preSer) (117.5 mg, 450 μmol) in 10 ml of anhydrous *N*,*N*′-dimethylformamide (DMF) was added with TSTU (136.4 mg, 450 μmol). After the solution was stirred for 15 min, *N*,*N*-diisopropylethylamine (DIPEA; 78 μl, 450 μmol) was added, and the resulting solution was stirred for 4 hours. A solution of chitosan with a molecular weight of 2.5 kDa (250 mg, 100 μmol) in 10 ml of deionized water was added to the reaction to obtain a clear solution. The solution was stirred at room temperature for 12 hours and then purified by dialysis [molecular weight cutoff (MWCO), 2.0 kDa] against deionized water for 2 days, followed by lyophilization. The products were dissolved in a TFA cocktail (95% TFA, 2.5% TIS, and 2.5% water) to deprotect the boc and tBu groups. The reaction mixtures were incubated at room temperature for 30 min. After completion of deprotection, this solution was evaporated to remove most of TFA. The residue was purified by dialysis (MWCO, 2.0 kDa) against deionized water for 2 days, followed by lyophilization.

To synthesize PEG-C, mPEG-COOH (240 mg, 120 μmol) was dialyzed in 10 ml of anhydrous DMF, was added with TSTU (36.4 mg, 120 μmol) and DIPEA (21 μl, 120 μmol), and then stirred at room temperature for 4 hours. A solution of chitosan (250 mg, 100 μmol) in 10 ml of deionized water was added to the reaction to obtain a clear solution. The solution was stirred at room temperature for 12 hours and then purified by dialysis (MWCO, 3.5 kDa) against deionized water for 2 days, followed by lyophilization.

L-Serine was conjugated with chitosan through PEG to synthesize S-PEG-C. A solution of preSer (31.3 mg, 120 μmol) in 2 ml of anhydrous DMF was added with TSTU (36.4 mg, 120 μmol). After the solution was stirred for 15 min, DIPEA (21 μl, 120 μmol) was added, and the resulting solution was stirred for 4 hours. NH_2-PEG-COOH (240 mg, 120 μmol) was added to the reaction, and the solution was further stirred for another 8 hours at room temperature. TSTU (36.4 mg, 120 μmol) and DIPEA (21 μl, 120μmol) were added. A solution of chitosan with a molecular weight of 2.5 kDa (250 mg, 100 μmol) in 10 ml of deionized water was added to the reaction to obtain a clear solution. The solution was stirred at room temperature for 12 hours and then purified by dialysis (MWCO, 3.5 kDa) against deionized water for 2 days, followed by lyophilization. The products were deprotected by TFA cocktail and purified by dialysis (MWCO, 3.5 kDa) against deionized water for 2 days, followed by lyophilization.

SC, PEG-C, and S-PEG-C were identified using ^{1}H NMR spectroscopy (AC-80, Bruker Biospin, Germany) in deuterated water. According to the area of characteristic peaks, the ratio of substitution of these macromolecules was calculated, and the molecular weight was speculated. The molecular weight of SC was analyzed using GPC.

Synthesis of Cy5-labeled chitosan-based materials

Chitosan (2.0 ml, 2 mg/ml, 1.6 μM, water), SC (2.0 ml, 2.5 mg/ml, water), PEG-C (2.0 ml, 4 mg/ml, water), or S-PEG-C (2.0 ml, 4 mg/ml, water) was mixed with Cy5-NHS (1.2 mg, 1.6 μM) and stirred at room temperature overnight. The product was purified by dialysis against deionized water for 24 hours, followed by lyophilization.

Induction of IR-induced AKI and screening of formulations

Institute of Cancer Research (ICR) mice (male, 6 to 8 weeks old, 20 to 25 g) were purchased from Zhejiang Academy of Medical Sciences (Hangzhou, China). All animal experiments were performed in accordance with the National Institutes of Health Guide for the Care and Use of Laboratory Animals with the approval of the Scientific Investigation Board of Zhejiang University, Hangzhou, China. ICR mice were anesthetized by intraperitoneal administration of 1% pentobarbital sodium at a dose of 50 mg/kg. Renal ischemia was induced by clamping of the bilateral renal pedicles. During the ischemic period, body temperature was maintained by placing the mice on a 37°C heating table. After 30 min, both clamps were released, and mice were received administration intravenously. Moreover, to determine the role of SC in targeting to the AKI-injured kidney, mice were randomly divided into (i) the C group, in which the mice were subjected to renal IR and then given Cy5-C (0.2 ml, at a dose of 20 mg/kg); (ii) the PEG-C group, in which the mice were subjected to renal IR and then given Cy5-PEG-C (0.2 ml, at a dose of 40 mg/kg); (iii) the S-PEG-C group, in which the mice were subjected to renal IR and then given Cy5-S-PEG-C (0.2 ml, at a dose of 40 mg/kg); and (iv) the SC group, in which the mice were subjected to renal IR and then given SC (0.2 ml, at a dose of 25 mg/kg). At 4 or 12 hours after reperfusion, mice were euthanized, and main organs including the heart, lung, liver, spleen, and kidney were harvested for fluorescence visualization. The healthy mice were administrated and processed as mentioned above. The organs were visualized by the Maestro In Vivo Imaging System (Cambridge Research & Instrumentation Inc., Woburn, MA, USA), and the relative fluorescence intensity was calculated in the same system.

The kidney sections of AKI-injured ICR mice were acquired 4 hours after intravenous injection of Cy5-SC at a concentration of 25 mg/kg and visualized by confocal microscopy.

Immunofluorescence staining

ICR mice were subjected to renal IR and then given Cy5-SC. At 4 hours and after reperfusion, mice were euthanized, and kidneys were harvested. Kidney sections were stained with fluorescent LTL for 1 hour to label proximal tubules. For labeling Kim-1, the slides were exposed to the primary antibodies [anti–Kim-1 (1:200; GeneTex)] and then to fluorescein isothiocyanate (FITC)–labeled secondary antibodies. Renal sections were also treated with DAPI. The staining was examined using fluorescence microscopes.

Synthesis and characteristics of SC-TK-SS31 and other SS31 prodrugs

SS31 was conjugated with SC through TK linkages to synthesize SS31-conjugated SC, with irresponsive linker (nonane diacid) as control (fig. S1). TK linker was synthesized according to the previous report (*40*). A mixture of anhydrous 3-mercaptopropionic acid (5.2 g, 49.1 mmol), anhydrous acetone (5.8 g, 98.2 mmol), and catalytic amount of TsOH was stirred for 6 hours at room temperature. Then, the reaction was quenched by placing the mixture on ice until the crystallization was complete. The crystals were filtered, washed with hexane and cold water three times, and dried in a vacuum dryer to obtain the product.

The primary amino group of SS31 was coupled to the carboxyl of TK linker through an amination reaction to obtain SS31-TK-NHS. Briefly, TK linker (10.2 mg, 37 μmol) in 10 ml of anhydrous DMF was mixed with TSTU (12.3 mg, 41 μmol). After the solution was stirred for 15 min, DIPEA (7 μl, 41 μmol) was added, and the resulting solution was stirred for 4 hours. SS31 (20 mg, 31.3 μmol) was added to the reaction, and the solution was stirred at room temperature for 12 hours and then purified by dialysis (MWCO, 500 Da) against deionized water for 2 days, followed by lyophilization. Irresponsive linker (nonane diacid) was also used to synthesize SS31-NO-NHS by a similar protocol. The successful syntheses of SS31-TK-NHS

and SS31-NO-NHS were confirmed by the appearance of peaks at ~6.4 ppm (attributed to the protons of aromatic ring in SS31), peaks at ~2.6 and ~ 2.8 ppm (attributed to methylene groups in TK), or peaks at ~1.4 ppm (attributed to methylene groups in NO) in ^{1}H NMR spectra. ^{13}C NMR spectra also assisted to confirm the successful syntheses of SS31-TK-NHS and SS31-NO-NHS by the appearance of peaks at ~128 ppm (attributed to the carbons of aromatic ring in SS31), peaks at ~35 ppm (attributed to carbons of methylene groups in TK), or peaks at ~25 ppm (attributed to carbons of methylene groups in NO; fig. S2).

preSC-TK-SS31 was synthesized by conjugating SS31-TK-NHS to preSC. Briefly, SS31-TK-NHS (20 mg, 22 μmol) was dissolved in 5 ml of DMF at room temperature and mixed with TSTU (7.3 mg, 24 μmol). After the solution was stirred for 15 min, DIPEA (4 μl, 23 μmol) was added. A solution of preSC (60 mg, 20 μmol) in 5 ml of deionized water was then added to the reaction to obtain a clear solution. The solution was stirred at room temperature for 24 hours and then purified by dialysis (MWCO, 2 kDa) against deionized water for 2 days, followed by lyophilization. Untargeted and irresponsive SS31 prodrugs, C-TK-SS31 and preSC-NO-SS31 were also synthesized by a similar protocol. The deprotection of boc and tBu groups used the same method as mentioned before.

C-TK-SS31, SC-NO-SS31, and SC-TK-SS31 and the intermediates were identified using ^{1}H-NMR spectroscopy in deuterated water. According to the area of characteristic peaks, the ratio of substitution of these macromolecules was calculated, and drug loading amount was speculated. The molecular weight of SC-TK-SS31 was analyzed using GPC.

Synthesis of fluorescent SS31 prodrugs

SS19 is the fluorescent analog of SS31 with an excitation and emission wavelength at 320 and 420 nm, respectively. SC-TK-SS19 and Ser-NO-SS19 were synthesized in the same method with SC-TK-SS31 by replacing SS19 with SS31. Cy5-SC-TK-SS19 or Cy5-SC-NO-SS19 was performed using the same method described above.

Plasma stability of SS31 and SC-TK-SS31

To investigate the stability of SC-TK-SS31 in plasma, SC-TK-SS31 was incubated with plasma of mice at a concentration of SS31 (10 μg/ml) in a 37°C incubator for 24 hours, with free SS31 as control. The plasma level of remaining SS31 was quantified by HPLC referring the published papers (*41*). The plasma samples were deproteinated with CH_3CN. The filtered plasma samples were collected at the same volume, dried, and then resolved in double-distilled (DD) water with H_2O_2 (100 mM) for concentration. SS31 was quantified by HPLC with a C18 column. Acetonitrile/water with 0.1% TFA (25:75, v/v) was used as the mobile phase. The column temperature and the detection wavelength were 25°C and 220 nm with a flow rate at 1.0 ml/min and an injection volume of 20 μl.

H_2O_2-triggered cleavage of TK linker

The cleavage of TK in SC-TK-SS31 were investigated by incubating SC-TK-SS31 (1 mg) in 500-μl release medium [phosphate-buffered saline (PBS), 0.01 M (pH 7.4)] with H_2O_2 (10 mM) at 37°C, referring the published papers (*42*–*46*). At designed time intervals, the mixture was detected by HPLC to monitor the cleavage of SC-TK-SS31 with a C18 column. SC-NO-SS31 was treated with the same protocol as control. Acetonitrile/water with 0.1% TFA (21:79, v/v) was used as the mobile phase. The column temperature and the detection wavelength were 25°C and 220 nm with a flow rate at 1.0 ml/min and an injection volume of 20 μl. HPLC-MS (6546 LC/Q-TOF) was used for evaluating released components of SC-TK-SS31 after incubation with H_2O_2 (10 mM) for 48 hours. The different contents of SC-TK-SS31, including SS31, Boc-Ser(tBu)-OH, C and SC, as along with SC-TK-SS31 at a concentration of 1 mg/ml were detected about UV and visible absorbance at wavelength from 200 to 500 nm by UV and visible spectrophotometer (UV-2600, SHIMADZU).

Cell culture

HK-2 cells were cultured in Dulbecco's modified Eagle's medium (DMEM)/nutrient mixture F-12 (DMEM/F12) with 10% fetal bovine serum and 1% penicillin/streptomycin in a 37°C cell incubator with 5% CO_2.

In vitro cytotoxicity tests for SC

For the in vitro cytotoxicity test, HK-2 cells were plated in 96-well plates. After the cells reached 80% confluency, they were treated with SC and chitosan with concentrations ranging from 0 to 500 μg/ml for 24 hours. MTT was used to evaluate cell viability.

Uptake by H_2O_2-stimulated HK-2 cells

HK-2 cells were seeded into 12-well plates and incubated with H_2O_2 (500 μM) and different samples (Cy5-SC and Cy5-C at a concentration of 500 μg/ml) for a predetermined time (2 and 6 hours), referring published papers (*14*, *47*–*52*). After washing with PBS, the cells were harvested and tested by flow cytometry (ACEA NovoCyteTM, ACEA Biosciences, USA). Normal HK-2 cells were also tested as control.

Kim-1 targeting ability

To investigate the Kim-1–targeted cell uptake of SC, HK-2 cells were seeded into 12-well plates and incubated overnight. After previous stimulation with H_2O_2 (500 μM) for 4 hours, HK-2 cells were treated with a blocking antibody to Kim-1 at a concentration of 30 μg/ml for 0.5 hours and then administrated with different samples (Cy5-SC and Cy5-C at a concentration of 500 μg/ml) for another 4 hours. HK-2 cells expressing Kim-1 were stained with anti–Kim-1 (1:200; GeneTex) and then to FITC-labeled secondary antibodies. The staining was examined using CLSM (Zeiss LSM 510 META, Carl Zeiss, Germany). H_2O_2-stimulated cells without blocking treatment of Kim-1 antibody were also tested as control.

Drug release in vitro

HK-2 cells were seeded into 12-well plates and incubated overnight. Then, cells were treated with H_2O_2 (500 mM) and different samples (Cy5-SC-TK-SS19, Cy5-SC-NO-SS19, and free SS19) at a concentration of 500 μg/ml for a predetermined time (4 and 12 hours), and normal HK-2 cells were also tested as control. After washing with PBS and fixing with 4% formaldehyde solution, the fluorescence in cells was monitored using CLSM. The extent of overlay of fluorescence was analyzed by ImageJ.

Mitochondria targeting ability

HK-2 cells were treated with H_2O_2 (500 mM) and SC-TK-SS19 at a concentration of 500 μg/ml for 12 hours. Mitochondria were dyed with MitoTracker at a concentration of 250 ng/ml for 30 min. After washing with PBS, the fluorescence in cells were monitored using CLSM. Free SS19 was tested as control.

Mitochondrial ROS detection

To assess the mitochondrial ROS decrease in SC-TK-SS31, HK-2 were seeded into 12-well plates and incubated with H_2O_2 (500 μM) and different samples [SS31, C-TK-SS31, SC-NO-SS31, and SC-TK-SS31 at a concentration of SS31 (20 μg/ml)] for 24 hours. After washing with PBS three times, HK-2 cells were incubated with MitoSOX Red Mitochondrial Superoxide Indicator (5 μM) for 10 min. Thereafter, the mitochondrial ROS level was determined by CLSM. Normal cells or H_2O_2-stimulated cells without drug treatment were used as control groups.

Mitochondrial membrane potential

HK-2 cells were incubated with H_2O_2 (500 μM) and different samples [SS31, C-TK-SS31, SC-NO-SS31, and SC-TK-SS31 at a concentration of SS31 (20 μg/ml) for 24 hours and then incubated with culture medium containing JC-1 dye (10 μg/ml) for 15 min. The cells were washed with culture medium, incubated in fresh medium, and visualized under CLSM. JC-1 dyes were excited at 488 nm, detected at 535-nm emission for JC-1 monomers, excited at 550 nm, and detected at 600-nm emission for JC-1 aggregates.

Apoptosis detection in vitro

HK-2 cells were plated into 12-well plates and treated with different samples [SS31, C-TK-SS31, SC-NO-SS31, and SC-TK-SS31 at a concentration of SS31 (20 μg/ml)] for 24 hours. Then, HK-2 cells were harvested, resuspended in the buffer, incubated with annexin V–FITC, stained with propidium iodide (Beyotime Biotechnology Co. Ltd.), and examined using a flow cytometer. Flow cytometry was repeated in three independent experiments.

Western blot

HK-2 cells were lysed according to the lysis protocol in ice-cold radioimmunoprecipitation assay. The kidney tissues were homogenized in ice-cold phosphate buffer (10 mM) (pH 7.2). The concentration of protein was tested using a BCA protein assay kit. Equal amounts of proteins for each group were loaded on SDS–polyacrylamide gel electrophoresis gels (8% for Kim-1 and 12% for HO-1). Following electrophoresis, the membranes were then probed overnight at 4°C with primary antibodies for Kim-1 (1:2000) and for HO-1 (1:1000). After being washed, the membrane was incubated with appropriate secondary antibody (the secondary ant-rabbit IgG HRP; 1:1000) for 3 hours at room temperature. The secondary antibody was imaged using the chemical illuminant (BeyoECL Plus) and quantified in a Bio-Rad system (ChemiDoc Touch Imaging System).

Administration protocols for in vivo therapeutic evaluation

The method of inducting renal IR injury had been described above. Here, to determine the role of SC-TK-SS31 in IR-induced AKI, mice were randomly divided into (i) the sham-treated mice, in which the mice had identical surgical procedures without application of clamps; (ii) the AKI group, in which the mice were anesthetized and underwent surgery without any other treatment; (iii) the AKI + SS31 group, in which the mice were subjected to renal IR and then given SS31 (0.2 ml, 2mg/kg); (iv) the AKI + C-TK-SS31 group, in which the mice were subjected to renal IR and then given C-TK-SS31 [0.2 ml, at a dose of SS31 (2 mg/kg)]; (v) the AKI + SC-NO-SS31 group, in which the mice were subjected to renal IR and then given SC-NO-SS31 [0.2 ml, at a dose of SS31 (2 mg/kg)]; and (vi) the AKI + SC-TK-SS31 group, in which the mice were subjected to renal IR and then given SC-TK-SS31 [0.2 ml, at a dose of SS31 (2 mg/kg)]. At 48 hours after reperfusion, mice were euthanized, blood was drawn by enucleation of eyeball, and kidneys were harvested for histologic analysis.

Renal function and histology

Serum creatinine and BUN were determined by the Beckman Coulter AU5800 automatic biochemical analyzer (Contract with Beckman Coulter Inc., USA). Kidney histology was examined in formalin-fixed, H&E-stained sections. The degree of tubule damage was scored semiquantitatively on a 0 to 5 scale, according to the percentage of the outer medulla area affected by tubular necrosis and/or apoptosis, loss of brush border, hyaline casts, sloughed cells, and tubular dilation (0, no lesion; 1, <10%; 2, 10 to 25%; 3, 26 to 50%; 4, 51 to 75%; 5, >75%).

Oxidative stress and proinflammatory cytokines assay

The levels of GSH and MDA were examined using commercial kits according to the manufacturer's instructions. The levels of TNF-α and IL-6 were quantified using ELISA kits according to the manufacturer's procedures.

Electron microscopy

Renal tissues were fixed in 2.5% glutaraldehyde, then fixed in 1% osmium tetroxide, dehydrated in graded alcohols, and embedded in epoxy resin. Ultrathin sections were cut and stained with uranyl acetate and lead citrate and examined by TEM (JEOL JEM-1230, Japan).

Immunohistochemical staining for nitrotyrosine and macrophages

Deparaffinized and rehydrated renal tissue sections were blocked in blocking buffer for 30 min at room temperature, incubated with antinitrotyrosine or anti-CD68, and incubated with secondary antibodies of HRP-conjugated rabbit anti-mouse IgG. The average number of nitrotyrosine or $CD68^+$ cells was counted from five different fields of each sample.

TUNEL assay

Deparaffinized and rehydrated renal tissue sections were incubated with proteinase K for 20 min at room temperature. TUNEL labeling was then carried out according to the manufacturer's protocol. The number of positive cells was measured by counting five different fields from the outer medulla in each kidney examined.

Determination of SS31 concentration in main organs of AKI mice

The ICR mice subjected to renal IR were divided into (i) SS31 group, (ii) C-TK-SS31 group, and (iii) SC-TK-SS31 group. At 4 hours after injection of formulations at a dose of SS31 (2 mg/kg), mice were euthanized, and main organs (kidney, heart, lung, liver, and spleen) were harvested. The levels of SS31 in tissues were quantified by HPLC referring the published papers (*41*). Tissue homogenate samples were prepared and deproteinated with CH_3CN. The filtered sample were collected at the same volume, dried, and then resolved in DD water with H_2O_2 (100 mM) for concentration. SS31 was quantified by HPLC with a C18 column. The condition for HPLC was the same as that in plasma stability test.

SUPPLEMENTARY MATERIALS

Supplementary material for this article is available at http://advances.sciencemag.org/cgi/content/full/6/41/eabb7422/DC1

View/request a protocol for this paper from *Bio-protocol*.

REFERENCES AND NOTES

1. L. S. Chawla, P. W. Eggers, R. A. Star, P. L. Kimmel, Acute kidney injury and chronic kidney disease as interconnected syndromes. *N. Engl. J. Med.* **371**, 58–66 (2014).
2. R. Alobaidi, R. K. Basu, S. L. Goldstein, S. M. Bagshaw, Sepsis-associated acute kidney injury. *Semin. Nephrol.* **35**, 2–11 (2015).
3. R. Bellomo, J. A. Kellum, S. M. Bagshaw, Normotensive ischemic acute renal failure. *N. Engl. J. Med.* **357**, 2205 (2007).
4. S. G. Coca, S. Singanamala, C. R. Parikh, Chronic kidney disease after acute kidney injury: A systematic review and meta-analysis. *Kidney Int.* **81**, 442–448 (2012).
5. E. A. J. Hoste, J. A. Kellum, N. M. Selby, A. Zarbock, P. M. Palevsky, S. M. Bagshaw, S. L. Goldstein, J. Cerdá, L. S. Chawla, Global epidemiology and outcomes of acute kidney injury. *Nat. Rev. Nephrol.* **14**, 607–625 (2018).
6. S. J. Han, H. T. Lee, Mechanisms and therapeutic targets of ischemic acute kidney injury. *Kidney Res. Clin. Pract.* **38**, 427–440 (2019).
7. Q. Chen, A. K. S. Camara, D. F. Stowe, C. L. Hoppel, E. J. Lesnefsky, Modulation of electron transport protects cardiac mitochondria and decreases myocardial injury during ischemia and reperfusion. *Am. J. Physiol. Cell Physiol.* **292**, C137–C147 (2007).
8. S. Tanaka, T. Tanaka, M. Nangaku, Hypoxia as a key player in the AKI-to-CKD transition. *Am. J. Physiol. Renal Physiol.* **307**, F1187–F1195 (2014).
9. J. L. Martin, A. V. Gruszczyk, T. E. Beach, M. P. Murphy, K. Saeb-Parsy, Mitochondrial mechanisms and therapeutics in ischaemia reperfusion injury. *Pediatr. Nephrol.* **34**, 1167–1174 (2019).
10. E. Y. Plotnikov, A. V. Kazachenko, M. Y. Vyssokikh, A. K. Vasileva, D. V. Tcvirkun, N. K. Isaev, V. I. Kirpatovsky, D. B. Zorov, The role of mitochondria in oxidative and nitrosative stress during ischemia/reperfusion in the rat kidney. *Kidney Int.* **72**, 1493–1502 (2007).
11. H. H. Szeto, S. Liu, Y. Soong, D. Wu, S. F. Darrah, F.-Y. Cheng, Z. Zhao, M. Ganger, C. Y. Tow, S. V. Seshan, Mitochondria-targeted peptide accelerates ATP recovery and reduces ischemic kidney injury. *J. Am. Soc. Nephrol.* **22**, 1041–1052 (2011).
12. H. H. Szeto, First-in-class cardiolipin-protective compound as a therapeutic agent to restore mitochondrial bioenergetics. *Br. J. Pharmacol.* **171**, 2029–2050 (2014).
13. M. T. Sweetwyne, J. W. Pippin, D. G. Eng, K. L. Hudkins, Y. A. Chiao, M. D. Campbell, D. J. Marcinek, C. E. Alpers, H. H. Szeto, P. S. Rabinovitch, S. J. Shankland, The mitochondrial-targeted peptide, SS-31, improves glomerular architecture in mice of advanced age. *Kidney Int.* **91**, 1126–1145 (2017).
14. B. J. Bruno, G. D. Miller, C. S. Lim, Basics and recent advances in peptide and protein drug delivery. *Ther. Deliv.* **4**, 1443–1467 (2013).
15. J. Rautio, H. Kumpulainen, T. Heimbach, R. Oliyai, D. Oh, T. Järvinen, J. Savolainen, Prodrugs: Design and clinical applications. *Nat. Rev. Drug Discov.* **7**, 255–270 (2008).
16. K. Berger, J.-M. Bangen, L. Hammerich, C. Liedtke, J. Floege, B. Smeets, M. J. Moeller, Origin of regenerating tubular cells after acute kidney injury. *Proc. Natl. Acad. Sci. U.S.A.* **111**, 1533–1538 (2014).
17. M. E. M. Dolman, S. Harmsen, G. Storm, W. E. Hennink, R. J. Kok, Drug targeting to the kidney: Advances in the active targeting of therapeutics to proximal tubular cells. *Adv. Drug Deliv. Rev.* **62**, 1344–1357 (2010).
18. D. W. Lee, C. Lim, J. N. Israelachvili, D. S. Hwang, Strong adhesion and cohesion of chitosan in aqueous solutions. *Langmuir* **29**, 14222–14229 (2013).
19. R. C. F. Cheung, T. B. Ng, J. H. Wong, W. Y. Chan, Chitosan: An update on potential biomedical and pharmaceutical applications. *Mar. Drugs* **13**, 5156–5186 (2015).
20. S. Matsuura, H. Katsumi, H. Suzuki, N. Hirai, H. Hayashi, K. Koshino, T. Higuchi, Y. Yagi, H. Kimura, T. Sakane, A. Yamamoto, L-Serine-modified polyamidoamine dendrimer as a highly potent renal targeting drug carrier. *Proc. Natl. Acad. Sci. U.S.A.* **115**, 10511–10516 (2018).
21. T. Ichimura, E. J. P. V. Asseldonk, B. D. Humphreys, L. Gunaratnam, J. S. Duffield, J. V. Bonventre, Kidney injury molecule-1 is a phosphatidylserine receptor that confers a phagocytic phenotype on epithelial cells. *J. Clin. Invest.* **118**, 1657–1668 (2008).
22. G. J. Freeman, J. M. Casasnovas, D. T. Umetsu, R. H. DeKruyff, *TIM* genes: A family of cell surface phosphatidylserine receptors that regulate innate and adaptive immunity. *Immunol. Rev.* **235**, 172–189 (2010).
23. S. Wang, G. Yu, Z. Wang, O. Jacobson, L.-S. Lin, W. Yang, H. Deng, Z. He, Y. Liu, Z.-Y. Chen, X. Chen, Enhanced antitumor efficacy by a cascade of reactive oxygen species generation and drug release. *Angew. Chem. Int. Ed. Engl.* **58**, 14758–14763 (2019).
24. Y. Zhang, Q. Guo, S. An, Y. Lu, J. Li, X. He, L. Liu, Y. Zhang, T. Sun, C. Jiang, ROS-switchable polymeric nanoplatform with stimuli-responsive release for active targeted drug delivery to breast cancer. *ACS Appl. Mater. Interfaces* **9**, 12227–12240 (2017).
25. N. Ponnuswamy, M. M. C. Bastings, B. Nathwani, J. H. Ryu, L. Y. T. Chou, M. Vinther, W. A. Li, F. M. Anastassacos, D. J. Mooney, W. M. Shih, Oligolysine-based coating protects DNA nanostructures from low-salt denaturation and nuclease degradation. *Nat. Commun.* **8**, 15654 (2017).
26. M. Malek, M. Nematbakhsh, Renal ischemia/reperfusion injury; from pathophysiology to treatment. *J. Renal Inj. Prev.* **4**, 20–27 (2015).
27. D. P. Basile, M. D. Anderson, T. A. Sutton, Pathophysiology of acute kidney injury. *Compr. Physiol.* **2**, 1303–1353 (2012).
28. R. L. Chevalier, The proximal tubule is the primary target of injury and progression of kidney disease: Role of the glomerulotubular junction. *Am. J. Physiol. Renal.* **311**, F145–F161 (2016).
29. E. J. Sharples, Acute kidney injury: Stimulation of repair. *Curr. Opin. Crit. Care* **13**, 652–655 (2007).
30. K. Zhao, G.-M. Zhao, D. Wu, Y. Soong, A. V. Birk, P. W. Schiller, H. H. Szeto, Cell-permeable peptide antioxidants targeted to inner mitochondrial membrane inhibit mitochondrial swelling, oxidative cell death, and reperfusion injury. *J. Biol. Chem.* **279**, 34682–34690 (2004).
31. K. A. Nath, Heme oxygenase-1 and acute kidney injury. *Curr. Opin. Nephrol. Hypertens.* **23**, 17–24 (2014).
32. W. Van Biesen, R. Vanholder, N. Lameire, Defining acute renal failure: RIFLE and beyond. *Clin. J. Am. Soc. Nephrol.* **1**, 1314–1319 (2006).
33. R. Bellomo, J. A. Kellum, C. Ronco, Defining and classifying acute renal failure: From advocacy to consensus and validation of the RIFLE criteria. *Intensive Care Med.* **33**, 409–413 (2007).
34. E. Noiri, A. Nakao, K. Uchida, H. Tsukahara, M. Ohno, T. Fujita, S. Brodsky, M. S. Goligorsky, Oxidative and nitrosative stress in acute renal ischemia. *Am. J. Physiol. Cell Physiol.* **281**, F948–F957 (2001).
35. J. C. Jha, C. Banal, B. S. M. Chow, M. E. Cooper, K. Jandeleit-Dahm, Diabetes and kidney disease: Role of oxidative stress. *Antioxid. Redox Signal.* **25**, 657–684 (2016).
36. B. D. Sahu, M. Kuncha, G. J. Sindhura, R. Sistla, Hesperidin attenuates cisplatin-induced acute renal injury by decreasing oxidative stress, inflammation and DNA damage. *Phytomedicine* **20**, 453–460 (2013).
37. T. M. El-Achkar, M. Hosein, P. C. Dagher, Pathways of renal injury in systemic gram-negative sepsis. *Eur. J. Clin. Invest.* **38**, 39–44 (2008).
38. W. K. Han, V. Bailly, R. Abichandani, R. Thadhani, J. V. Bonventre, Kidney injury molecule-1 (KIM-1): A novel biomarker for human renal proximal tubule injury. *Kidney Int.* **62**, 237–244 (2002).
39. S. Arai, K. Kitada, T. Yamazaki, R. Takai, X. Zhang, Y. Tsugawa, R. Sugisawa, A. Matsumoto, M. Mori, Y. Yoshihara, K. Doi, N. Maehara, S. Kusunoki, A. Takahata, E. Noiri, Y. Suzuki, N. Yahagi, A. Nishiyama, L. Gunaratnam, T. Takano, T. Miyazaki, Apoptosis inhibitor of macrophage protein enhances intraluminal debris clearance and ameliorates acute kidney injury in mice. *Nat. Med.* **22**, 183–193 (2016).
40. Y. Yuan, J. Liu, B. Liu, Conjugated-polyelectrolyte-based polyprodrug: Targeted and image-guided photodynamic and chemotherapy with on-demand drug release upon irradiation with a single light source. *Angew. Chem. Int. Ed. Engl.* **53**, 7163–7168 (2014).
41. O. O. Grigoriants, J.-L. Tseng, R. R. Becklin, D. M. Desiderio, Mass spectrometric quantification of the mu opioid receptor agonist Tyr-D-Arg-Phe-Lys-NH_2 (DALDA) in high-performance liquid chromatography-purified ovine plasma. *J. Chromatogr. B Biomed. Sci. Appl.* **695**, 287–298 (1997).
42. D. Chen, G. Zhang, R. Li, M. Guan, X. Wang, T. Zou, Y. Zhang, C. Wang, C. Shu, H. Hong, L.-J. Wan, Biodegradable, hydrogen peroxide, and glutathione dual responsive nanoparticles for potential programmable paclitaxel release. *J. Am. Chem. Soc.* **140**, 7373–7376 (2018).
43. W. Zhang, X. Hu, Q. Shen, D. Xing, Mitochondria-specific drug release and reactive oxygen species burst induced by polyprodrug nanoreactors can enhance chemotherapy. *Nat. Commun.* **10**, 1704 (2019).
44. Q. Pei, X. Hu, X. Zheng, S. Liu, Y. Li, X. Jing, Z. Xie, Light-activatable red blood cell membrane-camouflaged dimeric prodrug nanoparticles for synergistic photodynamic/chemotherapy. *ACS Nano* **12**, 1630–1641 (2018).
45. W. Yin, W. Ke, N. Lu, Y. Wang, A. A.-W. M. M. Japir, F. Mohammed, Y. Wang, Y. Pan, Z. Ge, Glutathione and reactive oxygen species dual-responsive block copolymer prodrugs for boosting tumor site-specific drug release and enhanced antitumor efficacy. *Biomacromolecules* **21**, 921–929 (2020).
46. W. Ke, N. Lu, A. A.-W. M. M. Japir, Q. Zhou, L. Xi, Y. Wang, D. Dutta, M. Zhou, Y. Pan, Z. Ge, Length effect of stimuli-responsive block copolymer prodrug filomicelles on drug delivery efficiency. *J. Control. Release* **318**, 67–77 (2020).
47. Z. Guo, S. Kozlov, M. F. Lavin, M. D. Person, T. T. Paull, ATM activation by oxidative stress. *Science* **330**, 517–521 (2010).
48. V. Olin-Sandoval, J. S. L. Yu, L. Miller-Fleming, M. T. Alam, S. Kamrad, C. Correia-Melo, R. Haas, J. Segal, D. A. P. Navarro, L. Herrera-Dominguez, O. Méndez-Lucio, J. Vowinckel, M. Mülleder, M. Ralser, Lysine harvesting is an antioxidant strategy and triggers underground polyamine metabolism. *Nature* **572**, 249–253 (2019).
49. W.-J. Keune, D. R. Jones, Y. Bultsma, L. Sommer, X. Z. Zhou, K. P. Lu, N. Divecha, Regulation of phosphatidylinositol-5-phosphate signaling by Pin1 determines sensitivity to oxidative stress. *Sci. Signal.* **5**, ra86 (2012).

50. H.-S. Lee, C. Y. Hwang, S.-Y. Shin, K.-S. Kwon, K.-H. Cho, MLK3 is part of a feedback mechanism that regulates different cellular responses to reactive oxygen species. *Sci. Signal.* **7**, ra52 (2014).
51. E. Tapia, V. Soto, K. M. Ortiz-Vega, G. Zarco-Márquez, E. Molina-Jijón, M. Cristóbal-García, J. Santamaría, W. R. García-Niño, F. Correa, C. Zazueta, J. Pedraza-Chaverri, Curcumin induces Nrf2 nuclear translocation and prevents glomerular hypertension, hyperfiltration, oxidant stress, and the decrease in antioxidant enzymes in 5/6 nephrectomized rats. *Oxid. Med. Cell. Longev.* **2012**, 269039 (2012).
52. H.-F. Zhang, J.-H. Wang, Y.-L. Wang, C. Gao, Y.-T. Gu, J. Huang, J.-H. Wang, Z. Zhang, Salvianolic acid a protects the kidney against oxidative stress by activating the Akt/GSK-3β/Nrf2 signaling pathway and inhibiting the NF-κB signaling pathway in 5/6 nephrectomized rats. *Oxid. Med. Cell. Longev.* **2019**, 2853534 (2019).

Acknowledgments: We thank Jianyang Pan and Dan Wu (Research and Service Center,College of Pharmaceutical Sciences, Zhejiang University) for performing NMR and mass spectrometry for structure elucidation. **Funding:** This work was supported by National Natural Science Foundations of China (81874302 and 81671889) and Fundamental Research Funds for the Central Universities (2019QNA7032). **Author contributions:** Yongzhong Du, S.J., X.L., and D.L. designed the experiments. D.L., G.S., F.J., J.Q., X.X., Yan Du, H.Y., J.W., M.S., Y.Y., M.Z., M.C., L.Z., Q.S., and X.Y. performed the experiments. D.L. and G.S. analyzed the data and wrote the paper. **Competing interests:** The authors declare that they have no competing interests. **Data and materials availability:** All data needed to evaluate the conclusions in the paper are present in the paper and/or the Supplementary Materials. Additional data related to this paper may be requested from the authors.

Submitted 15 March 2020
Accepted 21 August 2020
Published 9 October 2020
10.1126/sciadv.abb7422

Citation: D. Liu, G. Shu, F. Jin, J. Qi, X. Xu, Y. Du, H. Yu, J. Wang, M. Sun, Y. You, M. Zhu, M. Chen, L. Zhu, Q. Shen, X. Ying, X. Lou, S. Jiang, Y. Du, ROS-responsive chitosan-SS31 prodrug for AKI therapy via rapid distribution in the kidney and long-term retention in the renal tubule. *Sci. Adv.* **6**, eabb7422 (2020).